Peer Review File

Helical dislocation-driven plasticity and flexible high-performance thermoelectric generator in α-Mg3Bi2 single crystals

Corresponding Author: Professor Jiaqing He

Parts of this Peer Review File have been redacted as indicated to remove third-party material.

This file contains all reviewer reports in order by version, followed by all author rebuttals in order by version.

Version 0:

Reviewer comments:

Reviewer #1

(Remarks to the Author)
In the manuscript "Helical dislocation-driven plasticity and flexible high-performance thermoelectric generator in α-Mg3Bi2 single crystals" by Mingyuan Hu et al., the authors reported the α-Mg3Bi2 single crystals as promising materials for flexible thermoelectric generators. The authors found that the α-Mg3Bi2 single crystals exhibit a high thermoelectric performance (with power factor up to 26.2 µW cm^-1K^-2) and high flexibility (with deformability factor up to 0.08 Gpa^-1), which makes them suitable for use in flexible thermoelectric generators. The authors also observed the origin of high flexibility comes from the helical dislocation in the crystal. Overall, the authors demonstrated that α-Mg3Bi2 single crystals are promising materials for flexible thermoelectric generators. Since the α-Mg3Bi2 is cheaper than the common thermoelectric material, Bi2Te3, and can be flexible, it can be an important material for future thermoelectric devices. Thus, I can suggest the publication of this manuscript in the journal after they address the following comments:

1. Regarding the origin of this work, the authors should provide more information about the motivation behind this study. The α-Mg3Bi2 has been reported for supper high plasticity under compression [Nat. Commun. 15, 5108 (2024), Nature 631, 777-782 (2024)]. According to my understanding from the introduction, the authors mentioned that "Differently, in this study, we presented the strain-induced helical dislocation-driven interlayer slip of (0001) planes and the fine distortion structure around dislocations". However, they did not clearly define "helical dislocation" and "fine distortion" in the introduction. Does helical dislocation occur locally at a few places or globally in the crystal?

2. In Fig. 1c, why do the strain-stress curves increase linearly as an exponential function? This mechanical behavior is contrary to previous reports [Nat. Commun. 15, 5108 (2024), Nature 631, 777-782 (2024)]. When the crystal is failure under compression? Why, for the c-axis, does the strain-stress curve have a step-like behavior at a compression strain of 2%?

3. In Fig. 1d, the authors showed the bandgap of Mg3Bi2 is 0 eV as Au and Ti. So why the authors called Mg3Bi2 is a semiconductor?

4. For the section "Strain-induced interlayer slip and atomic-scale locally distorted structures", the authors should compare the results with previous reports for the interlayer slip and the mechanism illustration of the helical dislocation in Figs. 2g and 2h are not convincing for me. I suggest that the authors optimize this structure using the density functional theory (DFT) calculation, which was considered in the method section. Then, the authors can calculate the STM image of the optimized structure to compare with the experimental STM image in Fig. 2e.

5. How do the locally distorted structures and compression strain affect the transport properties such as electrical and thermal conductivities? Can the authors use a simple model, such as the band model, to explain this effect (such as how the band gap or effective mass changes and why)?

6. The font size of all figures, particularly the legend, is tiny. Please improve the quality of the figures. For example, why do we need the gradient background color in Fig. 1d? It makes the figure difficult to see.

Reviewer #2

(Remarks to the Author)
This paper investigates single-crystal alpha-Mg3Bi2 as flexible thermoecltric devices. The ZT values are moderate, but in a device configuration, functionality is demonstrated with decent power output. The paper could possibly be suitable for Nature Communications. However, major revisions are required.

1. The Supplementary information is difficult to assess. It is a long listing of figures with caption, but missing descriptive and explanatory text. The Supplementary information should be divided into section, with text sections presenting and explaining the figures, otherwise it is not really possible to follow most of it.

2. For the device, the paper is missing information on the p-type material. It is stated in the methods part that it is "p-type (AgCu)0.999Te0.69Se0.3S0.01 ingots" but this is the only information available. What is the structure and properties of the p-type material? How much of the performance is determined by the n-type and the p-type material? How would it compare to a unileg module (ie with a dummy p-type material and only the Mg3Bi2 being the active material)? There is a description of the synthesis and I see a few property measurements in the SI, but no information about the material itself (eg XRD or composition determination).

3. Please provide full details of the thermal conductivity measurements, including uncertainties. "The thermal conductivity was calculated by the fomula of kappa = D*Cp*rho, where the thermal diffusivity (D) was tested by Netzsch LFA 467 LT." How was Cp determined?

4. There is a concept confusion (also occurring in some parts of the literature), and a few inaccuracies. These points should be polished. "Plasticity" or "Ductility" means that the materials deform permanently (plastically) without fracture or cracking, i.e., ductility is the opposite of brittleness. Please do not confuse "plasticity" and "ductility" with mechanical flexibility, which means that the materials deform elastically (or quasielastically), and then revert to their original shape when the load is removed. This is different from a ductile material, which deforms permanently. Thus, if the material is deforming plastically, it should not be described as mechanically flexible. I believe that the explanation is that the material is indeed mechanically plastic, but the deformation remains in the elastic part of the stress-strain curve.

5. Avoid describing the materials as "plastic semiconductor" and any variation. "Plastic" here is easily misunderstood as "polymer" (which of course would make no sense). Use "ductile" or "mechanically flexible" instead, depending on what is meant.

6. The background and context of the work is generally accurate. However, In the introduction, recent reviews on flexible thermoelectrics should be mentioned,(say, Du et al "Flexible thermoelectric materials and devices" Applied Materials Today 12, 366 (2018) and Wang et al Flexible Thermoelectric Flexible Thermoelectric Materials and Generators: Challenges and Innovations, Advanced Materials 31, 1807916 (2019)). For Mg3Bi2, Sadowski et al. Appl. Phys. Lett. 120, 051901 (2022) might also be relevant.

7. Furthermore, it is essential to reference also earlier, original, key work on flexible fully inorganic thermoelectrics. For example, ductile/flexible AgS (Nature Materials 2018 and several follow up papers from the same group), CuI (Yang et al, Nature Communications 2017), Ca3Co4O9-based [Paul et al ACS Applied Materials & Interfaces 9, 25308 (2017) and ACS Applied Energy Materials 1, 2261 (2018), as well as several later papers by the same groups], and several CNT-composites (eg Nature Materials 2019, or the review by Blackburn et al Adv. Mater. 30 (2018) 1704386.).

Reviewer #3

(Remarks to the Author)
Mg3Bi2 is a very promising material for thermoelectrics. In this article, the authors demonstrate outstanding mechanical properties of Mg3Bi2 in terms of plasticity and deformability that is uncommon for inorganic semiconductors. This property is very relevant for the development of flexible (possibly wearable) thermoelectric generators (TEG) as the authors demonstrate themselves by fabricating a flexible TEG with a normalized power density of 8.1 uW/cm2·K2 at a temperature difference of 7.3 K.
The study is well-conducted providing a thorough insight into the atomistic nature of the plasticity of Mg3Bi2 combining high-resolution microscopy and theoretical calculations.
I therefore think that the article is suitable for publication in Nature Communications, after considering the following aspects:

1) It is well-known, and the authors also highlight it in their manuscript, that the stoichiometry (Mg-rich or Bi-rich) greatly affects the electrical properties of Mg3Bi2 (n-type or p-type). Does it also have an effect on the mechanical properties? I could not find whether the investigated mechanical properties are on Mg-rich or Bi-rich crystals. What is the stoichiometry of the different crystals employed?
2) The authors visualize microstrain induced by bending with atomic-resolution imaging (Figure 2). I wonder whether this would be visible by more-accessible techniques like powder XRD (peak broadening)?
3) For the fabrication of the f-TEG the authors cut "thin plates" from the single crystals, that are around 330 microns thick. In

literature, there are several reports on thin films (sub-micron) grown by sputtering or thermal evaporation. How does the thickness affect the thermoelectric and mechanical properties of the material?

Version 1:

Reviewer comments:

Reviewer #1

(Remarks to the Author)
I want to thank the authors for providing detailed answers and making the additional calculations in the revised manuscript. Almost all my requirements have been satisfied. I believe that the content of this manuscript has been improved; in particular, the authors have clarified the role of the iDPC method compared with the TEM method in the previous publications and also performed the AIMD simulations to understand the atomic structure. Thus, I suggest publishing this work as it is on Nat. Commun.

Reviewer #2

(Remarks to the Author)
The authors have addressed all comments from the three reviewers in a very thorough and complete manner. I am pleased to recommend this paper for publication in Nature Communications.

Reviewer #3

(Remarks to the Author)
The authors have appropriately answered all my previous comments. I have no further comments and recommend publication of the current manuscript.

Response to Reviewer Reports

Reviewer #1 (Remarks to the Author):

In the manuscript "Helical dislocation-driven plasticity and flexible high-performance thermoelectric generator in α-Mg$_3$Bi$_2$ single crystals" by Mingyuan Hu et al., the authors reported the α-Mg$_3$Bi$_2$ single crystals as promising materials for flexible thermoelectric generators. The authors found that the α-Mg$_3$Bi$_2$ single crystals exhibit a high thermoelectric performance (with power factor up to 26.2 µW cm^{-1} K^{-2}) and high flexibility (with deformability factor up to 0.08 Gpa^{-1}), which makes them suitable for use in flexible thermoelectric generators. The authors also observed the origin of high flexibility comes from the helical dislocation in the crystal. Overall, the authors demonstrated that α-Mg$_3$Bi$_2$ single crystals are promising materials for flexible thermoelectric generators. Since the α-Mg$_3$Bi$_2$ is cheaper than the common thermoelectric material, Bi$_2$Te$_3$, and can be flexible, it can be an important material for future thermoelectric devices. Thus, I can suggest the publication of this manuscript in the journal after they address the following comments:

Response: We would like to thank reviewer 1 for his/her much appreciating our work, and for the comments and suggestions as well. We have carefully taken the comments into consideration in preparing our revision.

Comment 1. Regarding the origin of this work, the authors should provide more information about the motivation behind this study. The α-Mg$_3$Bi$_2$ has been reported for supper high plasticity under compression [Nat. Commun. 15, 5108 (2024), Nature 631, 777-782 (2024)]. According to my understanding from the introduction, the authors mentioned that "Differently, in this study, we presented the strain-induced helical dislocation-driven interlayer slip of (0001) planes and the fine distortion structure around dislocations". However, they did not clearly define "helical dislocation" and "fine distortion" in the introduction. Does helical dislocation occur locally at a few places or globally in the crystal?

Response: Thanks a lot for the reviewer's suggestions. The high-performance and low-cost α-Mg$_3$Bi$_2$-based materials has been reported for supper high plasticity [Nat. Commun. 15, 5108 (2024); Nature 631, 777-782 (2024)], and are expected to drive the development of flexible electronics. Regarding the origin of plasticity in α-Mg$_3$Bi$_2$,

extensive exploration has been conducted, including microstructural characterization and theoretical calculations. Zhao et al. only used TEM to identify the prismatic slip system $\{1\bar{1}00\}\langle11\bar{2}0\rangle$ in trigonal α-Mg$_3$Bi$_2$ crystals, and simulated this slip process by DFT [Nature 631, 777-782 (2024)]. They also predicted the presence of numerous slip systems in α-Mg$_3$Bi$_2$ crystals, which is the fundamental reason behind its plasticity. In hexagonal structure metals, typical slip systems include basal slip system $\{0001\}\langle11\bar{2}0\rangle$, prismatic slip system $\{10\bar{1}0\}\langle10\bar{1}1\rangle$, and pyramidal slip system $\{10\bar{1}1\}$ $\langle11\bar{2}0\rangle$. In this work, we explored the basal slip system of α-Mg$_3$Bi$_2$ crystals in detail by using various methods. Unlike previous studies that relied on TEM and were limited to resolving the arrangement of heavy Bi atoms, our approach leverages the integrated differential phase contrast (iDPC) technique to successfully reveal the complete atomic structure, including the arrangements of both heavy Bi and light Mg atoms. The TEM results indicated the strain-induced helical dislocation-driven interlayer slip of (0001) planes as the microscopic mechanism of plastic deformation. Furthermore, the fine distortion structures around the helical dislocations, combined with ab initio molecular dynamics (AIMD) simulations and time-of-flight neutron diffraction analysis, revealed that the significant dispersion of lightweight Mg atoms plays a pivotal role in facilitating strain redistribution during plastic deformation. In conclusion, the plasticity of α-Mg$_3$Bi$_2$ stems from the helical dislocation-driven interlayer slip, small-sized Mg atoms induced weak interlayer Mg-Bi bonds, and low modulus of intralayer Mg$_2$Bi$_2^{2-}$ networks.

In addition, we thoroughly discussed the anisotropy of the thermoelectric properties for α-Mg$_3$Bi$_2$ crystals. We also fabricated an out-of-plane flexible thermoelectric generator, demonstrating that α-Mg$_3$Bi$_2$ crystals can be applied in flexible electronics. Our flexible thermoelectric generator leverages the performance along the c-axis, which is determined by the structure and mechanical properties in α-Mg$_3$Bi$_2$ crystals. The interlayer Mg1-Bi chemical bonds are relatively weak, and α-Mg$_3$Bi$_2$ easily dissociates along the ab-plane, as shown in the Fig. R1. When subjected to stress along the ab-plane, the samples are prone to dissociation (Fig. R1), leading to an open circuit in the device. Although the thermoelectric performance along the c-axis is not optimal, it is suitable for the out-of-plane devices. Ultimately, our out-of-plane flexible

thermoelectric generator exhibited a normalized power density of 8.1 μW cm^{-2} K^{-2} with a temperature difference of 7.3 K.

Fine structure generally refers to the detailed information of a sample at the micro- and nanoscale, including atomic positions, various structural defects, grain boundaries, and so on. In this work, by comparing the changes in the microstructure of the sample before and after deformation, it was found that the plasticity of α-Mg$_3$Bi$_2$ crystals originates from interlayer slip. During the slip process, helical dislocations are generated, and these dislocations drive the continuation of the slip. In this work, the crystal samples were repeatedly bent, and microstructural characterization of the deformed regions revealed the presence of many helical dislocations, as shown in Fig. 2 and Supplementary Fig. 9.
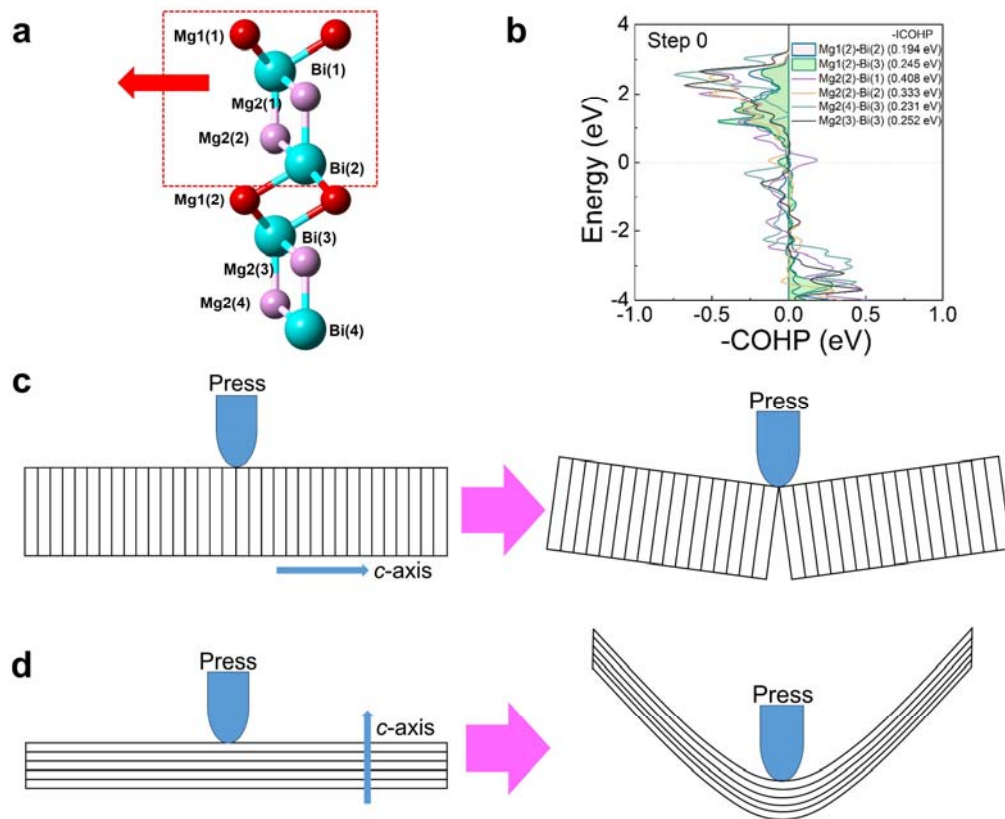

Fig. R1. a, The structure of α-Mg$_3$Bi$_2$. **b**, The crystal orbital Hamilton population (COHP) calculations in initial α-Mg$_3$Bi$_2$. The values of integrating the crystal orbital Hamilton population (-ICOHP) were also listed, which represent bond strength. (**c, d**) Fracture models under stress in different crystallographic directions for α-Mg$_3$Bi$_2$ crystal.

Comment 2. In Fig. 1c, why do the strain-stress curves increase linearly as an exponential function? This mechanical behavior is contrary to previous reports [Nat. Commun. 15, 5108 (2024), Nature 631, 777-782 (2024)]. When the crystal is failure under compression? Why, for the c-axis, does the strain-stress curve have a step-like behavior at a compression strain of 2%?

Response: Thank you for your suggestions. In a compression test, compressive stress (σ) is calculated by the formula ($\sigma=F/A$), where F refers to the force applied to the sample, and A is the area over which the force is applied. And the compressive strain (ε) is calculated by the formula ($\varepsilon=\Delta L/L_0$), where ΔL represents the deformation, and L_0 is the initial length of the sample. In Fig. R2a, the compressive stress value was the applied force divided by the initial cross-sectional area of the sample. However, as the deformation increased, the cross-sectional area also increased. In Fig. R2b, the cross-sectional area of the sample was calculated by the formula [$A=V/(L_0-\Delta L)$], and the compressive stress value was then the applied force divided by the updated cross-sectional area of the sample in compression test. Under compression stress, α-Mg$_3$Bi$_2$ crystals first undergoes a brief elastic stage (2%-4%), during which the samples could return to its original shape after the stress is removed. Once the stress exceeds the sample's yield strength, the samples began to undergo irreversible deformation, also known as plastic deformation. Notably, α-Mg$_3$Bi$_2$ crystals sustained >90% compression strain without cracking along the *ab*-plane and *c*-axis.
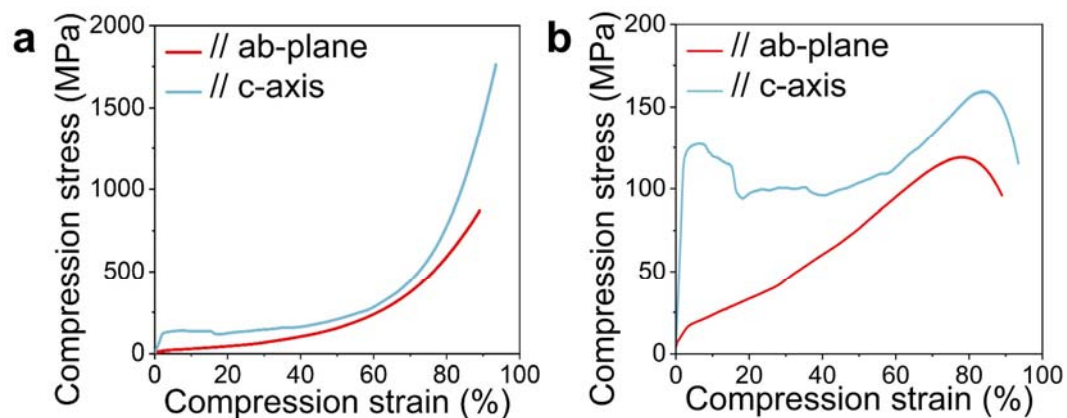

Fig. R2. a, The initial stress-strain curve of the uniaxial compression test. **b**, The optimized stress-strain curve of the uniaxial compression test.

Comment 3. In Fig. 1d, the authors showed the bandgap of Mg_3Bi_2 is 0 eV as Au and Ti. So why the authors called Mg_3Bi_2 is a semiconductor?

Response: Thanks for the reviewer's valuable comments. Mg_3Bi_2 is a topological nodal line semimetal with the coexistence of electron and hole pockets near Fermi level E_F [*Adv. Sci.* 6, 1800897 (2019)], as shown in Fig. R3. In this work, we also calculated the band structure of α-Mg_3Bi_2, as shown in Fig. R4, which is matched with the previous work [*Adv. Sci.* 6, 1800897 (2019)]. We have corrected this mistake in the manuscript.

[Figure redacted]

Fig. R3. Crystal structure and bulk bands of Mg_3Bi_2. (**a**) The lattice structure of Mg_3Bi_2; the blue and orange balls indicate the Mg and Bi atoms, respectively. (**b**) Powder X-ray diffraction (PXRD) pattern. The green arrows in the PXRD pattern correspond to the remaining Bi flux on the sample surface. (**c**) Bulk Brillouin zone and projected (001)-surface Brillouin zone. (**d**) Bulk band structure without the inclusion of spin–orbit coupling. (**e**) Bulk bands in part (**d**) with atomic orbital projection. (**f, g**) Same as parts (**d**) and (**e**) but with the inclusion of spin–orbit coupling. These results refer to Xie' work [*Adv. Sci.* 6, 1800897 (2019)].
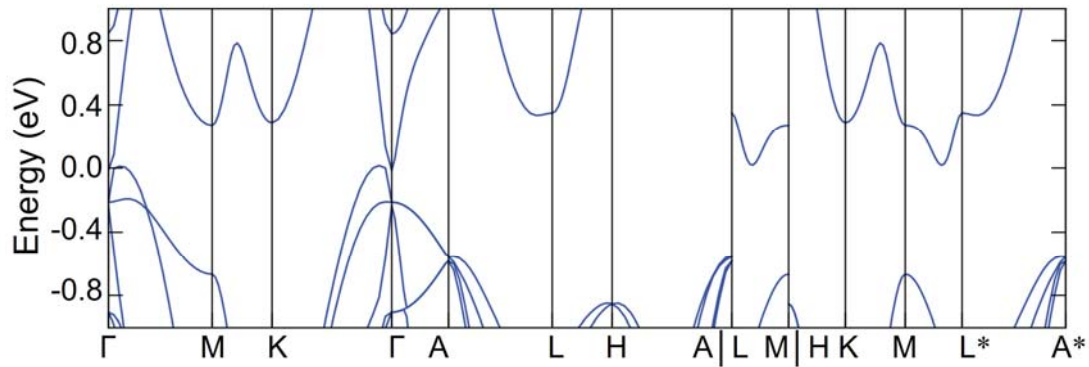
Fig. R4. The calculated band structure of α-Mg_3Bi_2 in this work.

Comment 4. For the section "Strain-induced interlayer slip and atomic-scale locally distorted structures", the authors should compare the results with previous reports for the interlayer slip and the mechanism illustration of the helical dislocation in Figs. 2g and 2h are not convincing for me. I suggest that the authors optimize this structure using the density functional theory (DFT) calculation, which was considered in the method section. Then, the authors can calculate the STM image of the optimized structure to compare with the experimental STM image in Fig. 2e.

Response: Thanks for the reviewer's valuable comments. Previous reports [*Nat. Commun.* 15, 5108 (2024); *Nature* 631, 777-782 (2024)] captured the edge dislocation-driven prismatic slip by using TEM technique, and analyzed basal, prismatic and pyramidal slip systems to explain the mechanism of plastic deformation for Mg_3Bi_2 crystal by DFT calculations. But the TEM results only showed the heavy Bi atomic arrangement in previous reports. In this work, we revealed the atomic arrangements of both heavy Bi and light Mg atoms by using integrated differential phase contrast (iDPC) technique. Our result indicated the helical dislocation-driven interlayer slip as the microscopic mechanism of plastic deformation. Moreover, the significant dispersion of light Mg atoms caused serious distortion of interlayer $MgBi_6$ and intralayer $MgBi_4$ polyhedra, which facilitated strain redistribution during plastic deformation.

To further clarify the slip process and compare it with our experimental results, we performed the ab initio molecular dynamics (AIMD) simulations, as illustrated in Figs. R5 and R6. The supercell of α-Mg_3Bi_2, containing 135 atoms, was optimized with layer slip distortion. As shown in Fig. R5b, the optimized supercell with distortion forms a specific helical dislocation, which results in a unique reorientation or flipping of the

atomic arrangement around the dislocation planes, as highlighted in the red circle. AIMD simulations were then carried out to analyze the evolution of the structure with helical dislocations in a supercell containing 540 atoms over time. After 20000 time steps of AIMD simulations at room temperature in the canonical ensemble (*NVT* ensemble), with a time step of 2 fs each, using the VASP code [*Phys. Rev. B* 54, 11169 (1996); *Comput. Mater. Sci.* 6, 1 (1996).], our results revealed that the atoms around the helical dislocation rearranged during the first 3,000 steps, and then the system ultimately equilibrated to a defect-free, perfect structure. A series of snapshots were captured throughout the simulation (Fig. R6), and two movies (Supplementary movies 2 and 3) were compiled to further analyze the structural changes. Herein, we also present four representative snapshots in Fig. R5. During the AIMD simulations, the heavier Bi atoms exhibited only small-amplitude vibrations, while the lighter Mg atoms showed large-amplitude vibrations, closely mirroring the experimental observations in Fig. 2g. Furthermore, the interlayer Mg atoms demonstrated a greater degree of dispersion compared to the intralayer Mg atoms, highlighting their more pronounced dynamic behavior within the structure. Both TEM and AIMD results confirm that helical dislocation-driven interlayer slipping processes lead to significant plastic deformation, serving as a microscopic mechanism of plastic deformation for α-Mg$_3$Bi$_2$. Additionally, the increased dispersed Mg atoms further facilitate the redistribution of strain throughout the plastic deformation process.

It is important to clarify that this study employed TEM (aberration-corrected transmission electron microscopy) to investigate the microscopic mechanisms of plastic deformation in the crystal, rather than STM (Scanning Tunneling Microscope). STM is primarily used to observe the surface structure of conductive materials, achieving atomic-level resolution. Unlike TEM, STM does not rely on transmitted electrons; instead, it collects surface morphology information through the tunneling current between a probe and the sample, making it more suitable for surface studies.
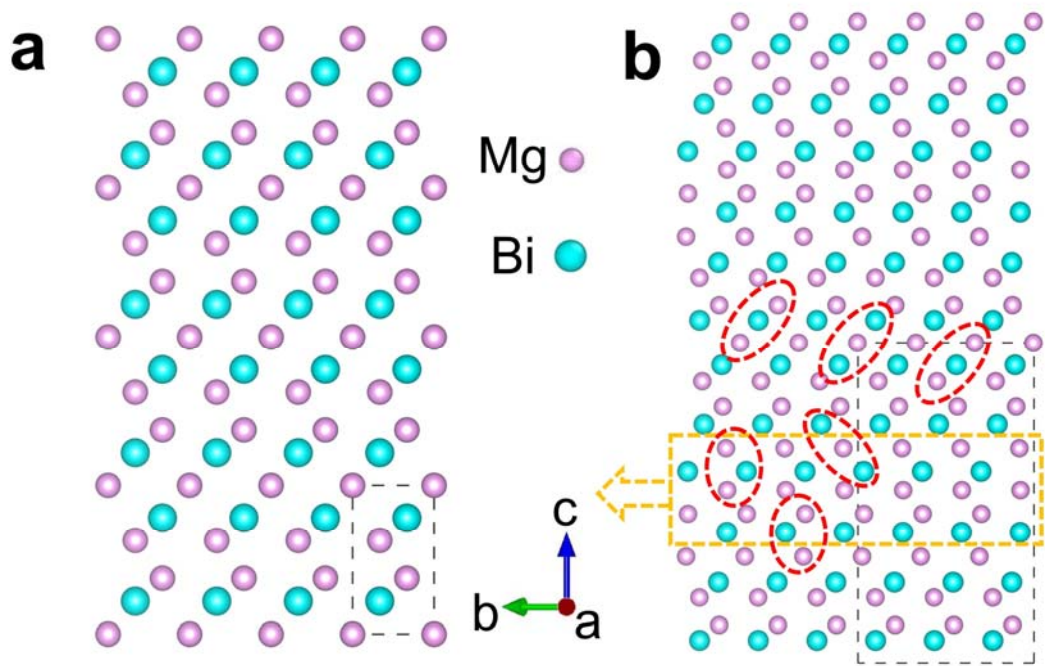
Fig. R5. a, the structure of α-Mg$_3$Bi$_2$ viewed along the $[10\bar{1}0]$. **b**, the optimized supercell of α-Mg$_3$Bi$_2$ with layer slip by half a cycle (the slip direction is indicated by yellow arrow).
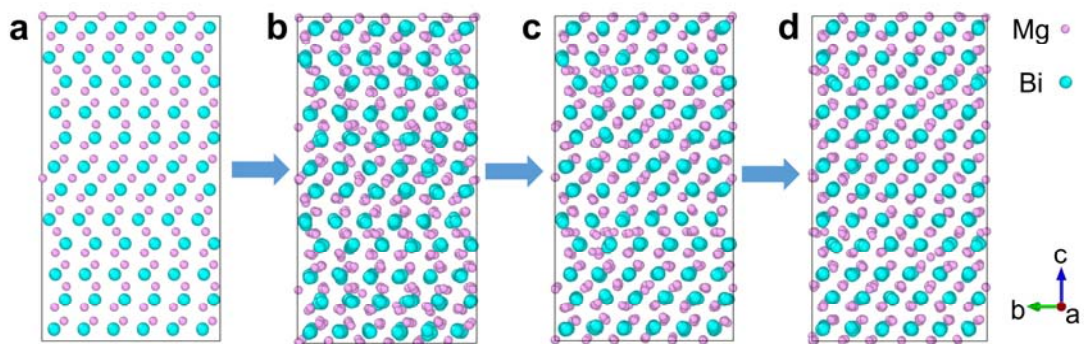

Fig. R6. a-d, The four representative snapshots of structure during the first 3000 steps from nonequilibrium state to equilibrium state in Ab initio molecular dynamics (AIMD) simulations.

Comment 5. How do the locally distorted structures and compression strain affect the transport properties such as electrical and thermal conductivities? Can the authors use a simple model, such as the band model, to explain this effect (such as how the band gap or effective mass changes and why)?

Response: Thanks for the reviewer's valuable comments. The effect of local structural distortion and compressive strain on transport properties is a very constructive suggestion. The band structure of α-Mg$_3$Bi$_2$ is calculated as shown in Fig. R7a. The conduction band minimum (CBM) is located at the Γ and C1 point (Fig. R7b and R7c) and the valence band maximum (VBM) is located at the O point (Fig. R7d). And the labeling of the reciprocal space and the Fermi surface for α-Mg$_3$Bi$_2$ are shown in Fig. R8. As shown in Fig. R8, the CBM are marked by blue, while the VBM are marked by purple. The conduction band is more dispersive along the U*→C1→U, and A*→Γ→A, and M*→Γ→M directions than that of the Δ→C1→Δ* directions. For the CBM at Γ point (Fig. R7b), the difference in the longitudinal ($0.059m_0$ along A*→Γ→A) and transverse ($0.048m_0$ along M*→Γ→M) electron effective mass is relatively small. For the CBM at C1 point (Fig. R7c), the longitudinal electron effective mass ($\sim 0.486m_0$ along Δ→C1→Δ*) is larger than that of the transverse electron effective masses ($\sim 0.124m_0$ along U*→C1→U). For the VBM, as shown in Fig. R7d and Fig. R8b, the values of the longitudinal and transverse hole effective mass are $0.467m_0$ along h→O→h* direction and $0.494m_0$ along K*→O→Γ direction, respectively.

The total electrical conductivity is jointly determined by the contribution of electrons and holes [J. Appl. Phys. **33**, 1830–1841 (1962); Mater. Today Phys. **22**, 100618 (2022); Nature **631**, 777-782 (2024)]

$$\sigma = n_e e \mu_e + n_h e \mu_h \tag{R1}$$

The electron concentration is

$$n_e = \frac{4\pi(2m_e^* k_B T)^{\frac{3}{2}}}{h^3} F_{\frac{1}{2}}(\eta_e) \tag{R2}$$

The hole concentration is

$$n_h = \frac{4\pi(2m_h^* k_B T)^{\frac{3}{2}}}{h^3} F_{\frac{1}{2}}(\eta_h) \tag{R3}$$

The electron mobility is

$$\mu_e = \frac{\sqrt{2}\pi e \hbar^4}{3(k_B T)^{3/2}} \frac{v_L^2 D}{\Xi^2 (m_e^*)^{3/2} m_c} \frac{F_0(\eta_e)}{F_{1/2}(\eta_e)} \tag{R4}$$

The hole mobility is

$$\mu_h = \frac{\sqrt{2}\pi e\hbar^4}{3(k_BT)^{3/2}} \frac{v_L^2 D}{\Xi^2 (m_h^*)^{3/2} m_c} \frac{F_0(\eta_h)}{F_{1/2}(\eta_h)} \tag{R5}$$

According to the Wiedemann-Franz rule, the electric thermal conductivity is

$$\kappa_e = L\sigma T \tag{R6}$$

Where, m_e^* and m_h^* is the density-of-states effective mass, and m_c is the conductivity effective mass. L is Lorentz constant. $F_i(\eta)$ is the Fermi integral. k_B and h are Boltzmann constant and Planck constant, respectively.
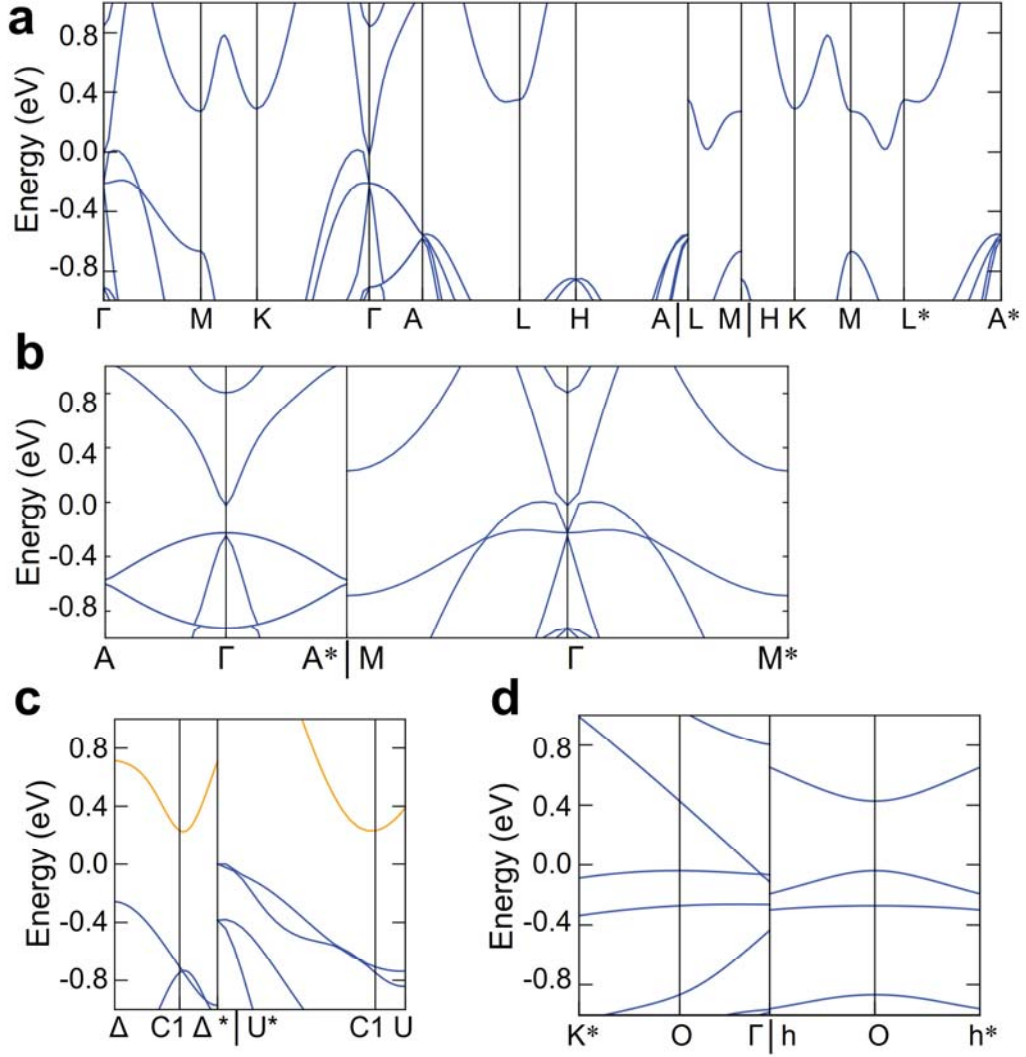

Fig. R7. a, The calculated band structure of α-Mg$_3$Bi$_2$. (**b, c**) The conduction band of α-Mg$_3$Bi$_2$ along different directions. **d**, The valence band of α-Mg$_3$Bi$_2$ along different directions.
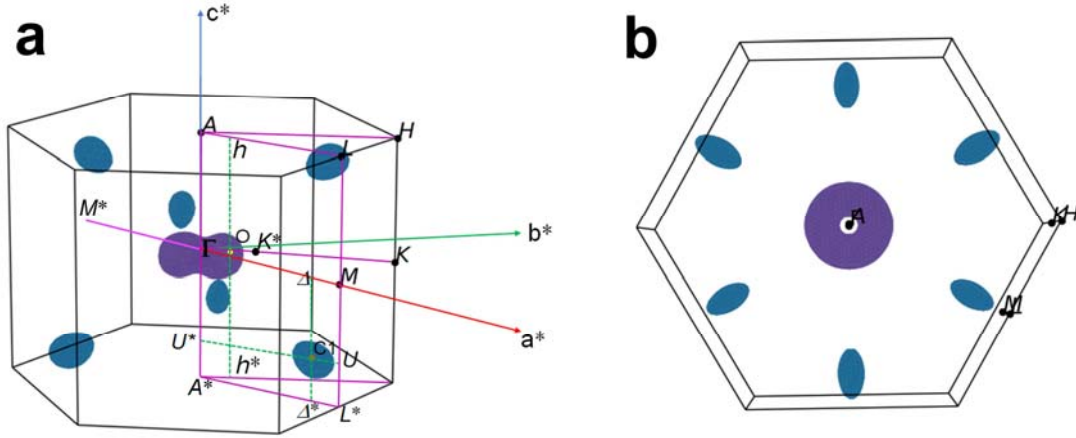
Fig. R8. a, The labeling of the reciprocal space and the iso-energy Fermi surface for α-Mg$_3$Bi$_2$. **b**, the iso-energy Fermi surface of α-Mg$_3$Bi$_2$ viewed from the A-Γ direction.

In order to study the effect of compressive strain on transport performance, the band structures of α-Mg$_3$Bi$_2$ are calculated under compression strain as shown in Fig. R9-R11. As the strain increases, the conduction band minimum and valence band maximum gradually separate, resulting in an increase of band gap values ($\sim$0.01eV) within 3% strain, as shown in Fig. R9-R11 and listed in Table R1. The trend of band gap changes under pressure is consistent with previous report [Nanomaterials **14**, 84 (2023)]. The value of the longitudinal electron effective mass along $\Delta\rightarrow$C1$\rightarrow\Delta^*$ direction gradually increases within 3% compression strain, which could lead to a decrease in electrical conductivity and electronic thermal conductivity along the c-axis, according to the formula R1, R2, R4, and R6. Moreover, the value of the transverse electron effective mass along M$^*\rightarrow\Gamma\rightarrow$M and U$^*\rightarrow$C1$\rightarrow$U directions change slightly, as listed in Table R1, which means that compression strain has a minimal impact on electrical conductivity and electronic thermal conductivity along ab-plane within 3% hydrostatic strain. In contrast, the hole effective masses gradually decrease under compression strain, which results in an increasing trend of electrical conductivity and electronic thermal conductivity, according to the formula R1, R3, R5, and R6. The smaller longitudinal hole effective masses could result in a larger electrical conductivity and electronic thermal conductivity along the c-axis.
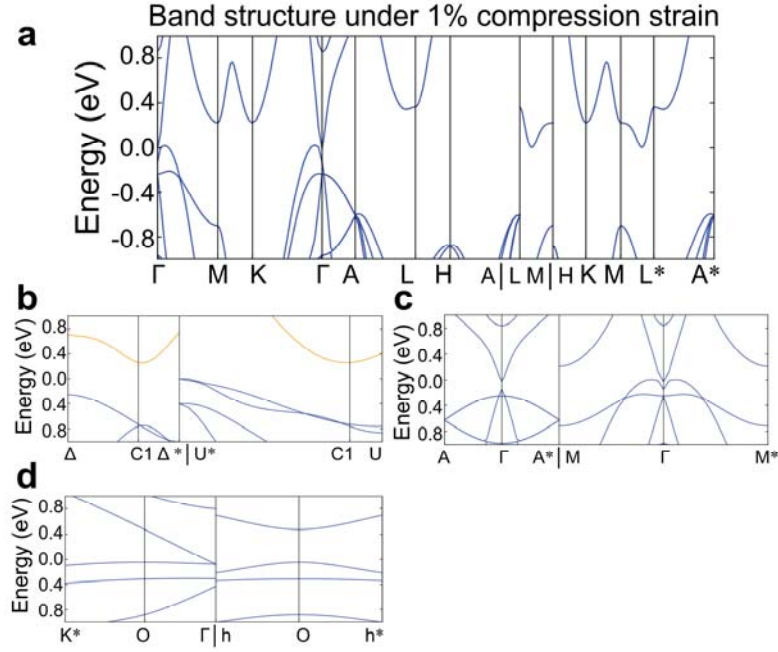
Fig. R9. a, The calculated band structure under isostatic pressure with 1% compression strain. The conduction band (**b, c**) and valence band (**d**) of α-Mg$_3$Bi$_2$ along different directions under 1% compression strain.

Fig. R10. a, The calculated band structure under isostatic pressure with 2% compression strain. The conduction band (**b, c**) and valence band (**d**) of α-Mg$_3$Bi$_2$ along different directions under 2% compression strain.
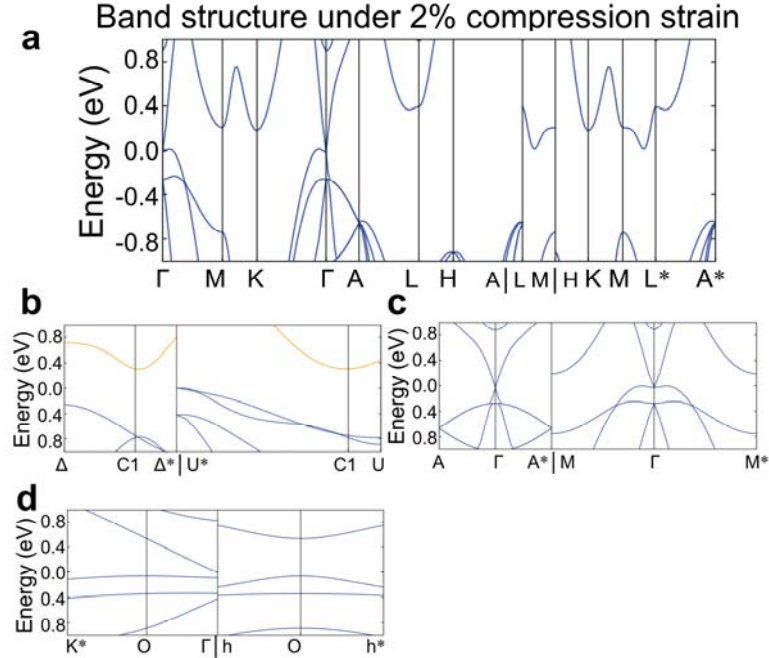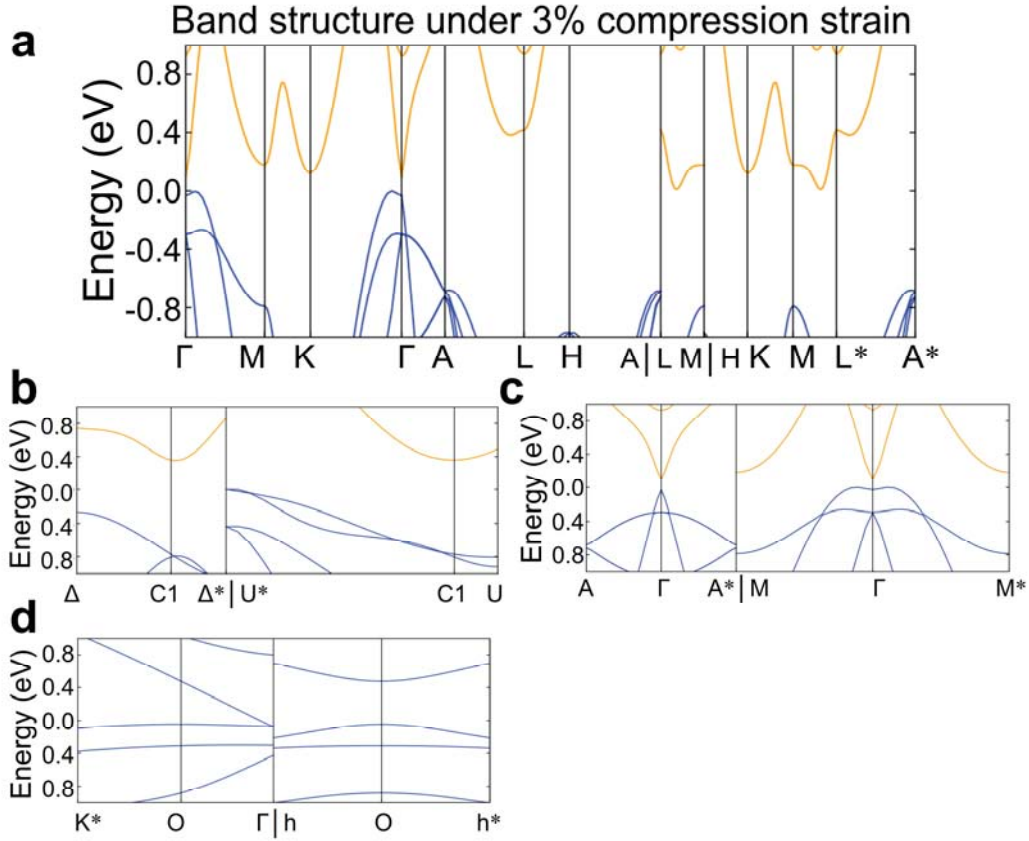
Fig. R11. a, The calculated band structure under isostatic pressure with 3% compression strain. The conduction band (**b, c**) and valence band (**d**) of α-Mg$_3$Bi$_2$ along different directions under 3% compression strain.

Table R1. The values of the band gap and effective mass under compression strain.

Band gap and effective mass under compression strain				
Strain	0	1%	2%	3%
Band gap (eV)	0	0	0	0.01
Effective mass (m_0)				
Valence Band Maximum (VBM)				
K*->O->Γ	0.494	0.464	0.450	0.439
h->O->h*	0.467	0.421	0.384	0.350
Conduction Band Minimum (CBM)				
Δ->C1->Δ*	0.486	0.589	0.757	1.073
U*->C1->U	0.124	0.130	0.125	0.126
A*->Γ->A	0.059	0.053	0.048	0.051
M*->Γ->M	0.048	0.047	0.052	0.053

The effect of local structural distortion on transport performance was also investigated. Since the local structural distortion was caused by shear strain, the band structures of α-Mg$_3$Bi$_2$ were calculated under shear stress as shown in Fig. R12-R14. As the shear strain increases, the value of band gap (~0.04 eV) also increased within 3% shear strain in Table R2, which is bigger than that under compression strain. The value of the longitudinal electron effective mass along $\Delta \rightarrow$ C1 $\rightarrow \Delta^*$ direction exhibits an overall decreasing trend, which could lead to an increase in electrical conductivity and electronic thermal conductivity along the c-axis, according to the formulas 3, 4, 6, and 8. Moreover, the value of the transverse electron effective masses along U$^* \rightarrow$ C1 $\rightarrow$ U and M$^* \rightarrow \Gamma \rightarrow$ M directions increase, as listed in Supplementary Table 10, which means that shear strain could lead to an decrease in electrical conductivity and electronic thermal conductivity along ab-plane within 3% shear strain. For VBM, the transverse hole effective mass changes slightly along K$^* \rightarrow$ O $\rightarrow \Gamma$ direction. In contrast, longitudinal hole effective mass decreases significantly from 0.467 to 0.095 along h $\rightarrow$ O $\rightarrow$ h* direction, which means an increasing trend of electrical conductivity and electronic thermal conductivity along c-axis.
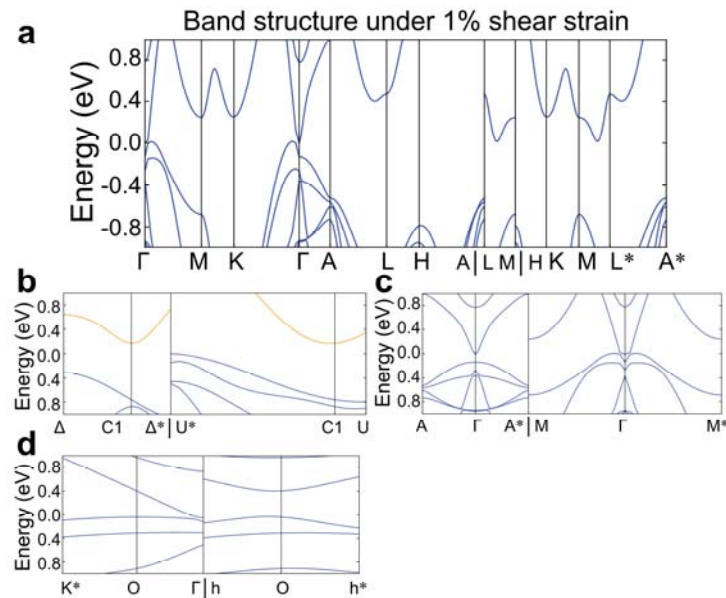

Fig. R12

a, The calculated band structure under 1% shear strain. The conduction band (**b, c**) and valence band (**d**) of α-Mg$_3$Bi$_2$ along different directions under 1% shear strain.

Fig. R13. a, The calculated band structure under 2% shear strain. The conduction band (**b**, **c**) and valence band (**d**) of α-Mg$_3$Bi$_2$ along different directions under 2% shear strain.

Fig. R14. a, The calculated band structure under 3% shear strain. The conduction band (**b**, **c**) and valence band (**d**) of α-Mg$_3$Bi$_2$ along different directions under 3% shear strain.
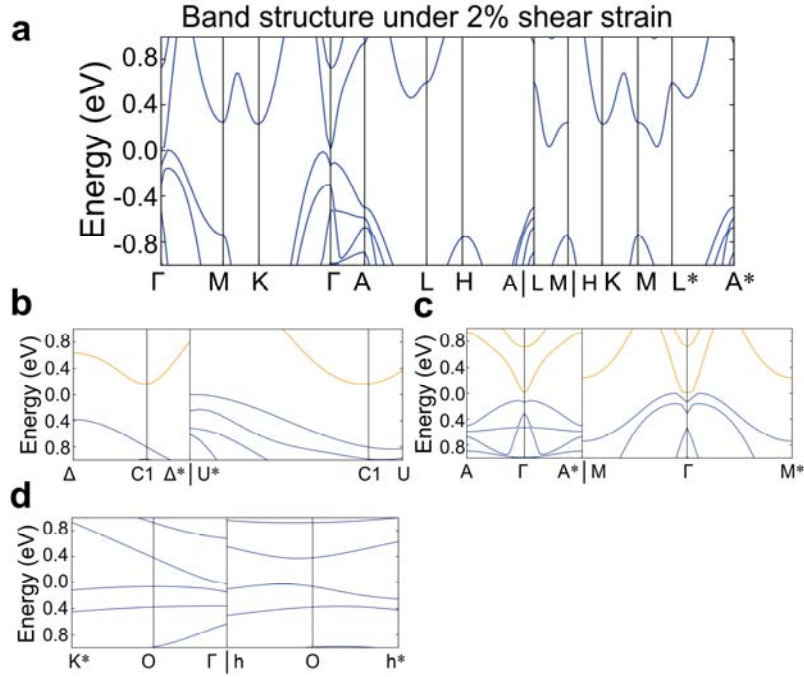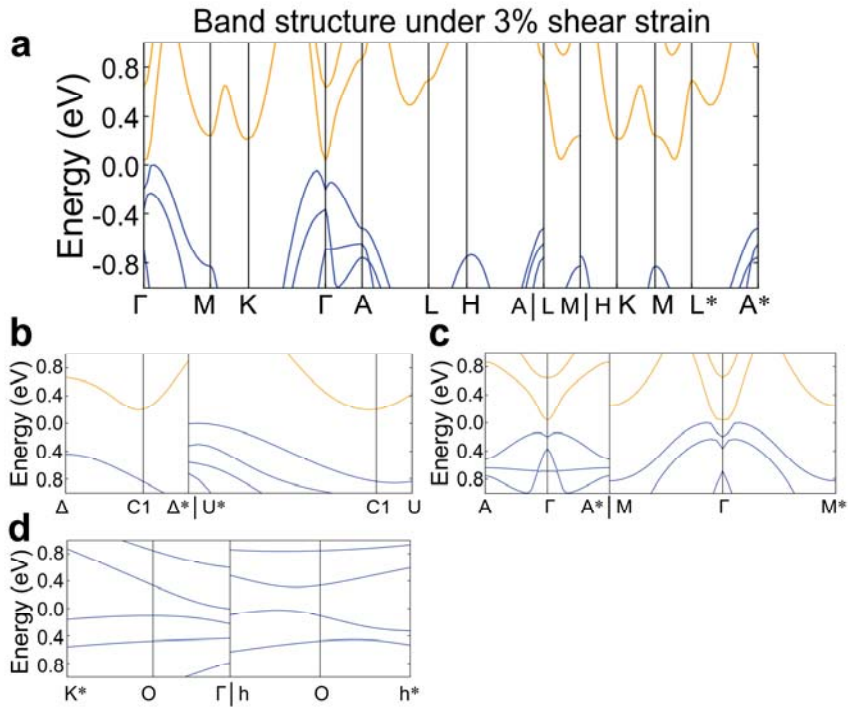**Table R2.** The values of the band gap and effective under shear stress.

Band gap and effective mass under shear stress				
Strain	0	1%	2%	3%
Band gap	0	0	0	0.04
Effective mass (m_0)				
Valence Band Maximum (VBM)				
K*->O->Γ	0.494	0.492	0.494	0.486
h->O->h*	0.467	0.272	0.152	0.095
Conduction Band Minimum (CBM)				
Δ->C1->Δ*	0.468	0.496	0.373	0.375
U*->C1->U	0.124	0.130	0.135	0.143
A*->Γ->A	0.059	0.062	0.071	0.088
M*->Γ->M	0.048	0.056	0.092	0.372

Comment 6. The font size of all figures, particularly the legend, is tiny. Please improve the quality of the figures. For example, why do we need the gradient background color in Fig. 1d? It makes the figure difficult to see.

Response: Thank you for your comments. I have refined the images to make them more accessible to readers.

Reviewer #2 (Remarks to the Author):

This paper investigates single-crystal alpha-Mg3Bi2 as flexible thermoecltric devices. The ZT values are moderate, but in a device configuration, functionality is demonstrated with decent power output. The paper could possibly be suitable for Nature Communications. However, major revisions are required.

Response: We would like to Reviewer 2 for his/her thoughtful review of our manuscript. We have carefully taken the comments into consideration in our revised manuscript.

Comment 1. The Supplementary information is difficult to assess. It is a long listing of figures with caption, but missing descriptive and explanatory text. The Supplementary information should be divided into section, with text sections presenting and explaining the figures, otherwise it is not really possible to follow most of it.

Response: Thank you for your suggestions. I have rearranged the supplementary material to make it easier for readers to access the information.

Comment 2. For the device, the paper is missing information on the p-type material. It is stated in the methods part that it is "p-type $(AgCu)0.999Te0.69Se0.3S0.01$ ingots" but this is the only information available. What is the structure and properties of the p-type material? How much of the performance is determined by the n-type and the p-type material? How would it compare to a unileg module (ie with a dummy p-type material and only the Mg3Bi2 being the active material)? There is a description of the synthesis and I see a few property measurements in the SI, but no information about the material itself (eg XRD or composition determination).

Response: Thanks for the reviewer's valuable suggestions. Owing to the poor thermoelectric performance of p-type α-Mg_3Bi_2 crystal, as shown in Supplementary Figs. 19 and 20, we chose another high-performance p-type $AgCu(Se, S, Te)$ pseudoternary solid solutions [Science 377, 854-858 (2022)] to fabricate the out-of-plane flexible thermoelectric generator. And by adjusting the ratio of raw materials and optimizing the process, we obtained the high-performance p-type plastic thermoelectric materials with higher power factor and zT value as shown in Supplementary Figs. 26. What's more, the powder XRD patterns for P-type $(AgCu)_{1-x}Te_{0.69}Se_{0.3}S_{0.01}$ ingots in this work matched with that for P-type $AgCu(Se, S, Te)$ pseudoternary solid solutions

[Science 377, 854-858 (2022)], as shown in Fig. R15. In the $(AgCu)_{0.999}Te_{0.69}Se_{0.3}S_{0.01}$ ingot, we obtained best thermoelectric performance with room-temperature zT value of 0.45, max zT value of 0.96 at 393 K, and the average zT value was 0.66 between 300-400 K. And the $(AgCu)_{0.999}Te_{0.69}Se_{0.3}S_{0.01}$ slab exhibited a bending strain greater than 17%, as shown in Fig. R16.

The as-prepared n-type α-Mg_3Bi_2 crystal and p-type $(AgCu)_{0.999}Te_{0.69}Se_{0.3}S_{0.01}$ ingots were cut into thin plates with the thickness about 330 μm by using the diamond wire cutting. The metallic barrier layers were both prepared for n-type and p-type materials by using spark plasma sintering (SPS- 211LX) at 773 K under a pressure of 50 MPa for 5 min, as shown in Supplementary Fig. 28. Then the plates were cut into square thermoelectric legs of 4×4 mm^2 by using the diamond wire cutting. The single-leg TEGs were fabricated by placing n-type and p-type legs between copper foils, as shown in Fig. R17a and R17b. For n-type single-leg TEG, the measured open circuit voltage (V_{oc}) and maximum output power (P_{max}) were 1.151 mV and 51.4 μW, respectively, under a temperature gradient (ΔT) of 12.1 K. While for p-type single-leg TEG, the measured open circuit voltage (V_{oc}) and maximum output power (P_{max}) were 2.43 mV and 147.7 μW, respectively, under a temperature gradient (ΔT) of 14.3 K. In a word, the output performance of the six-couple out-of-plane f-TEG, as shown in Fig. 5, benefits from the combined contributions of the n-type and p-type legs.
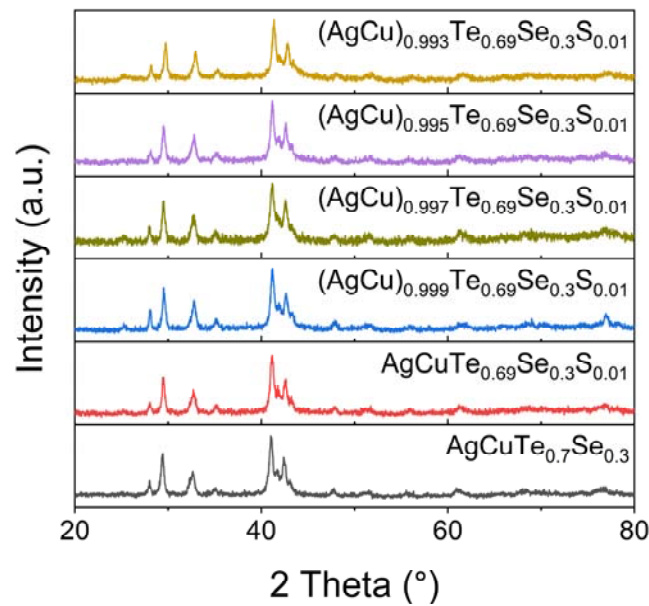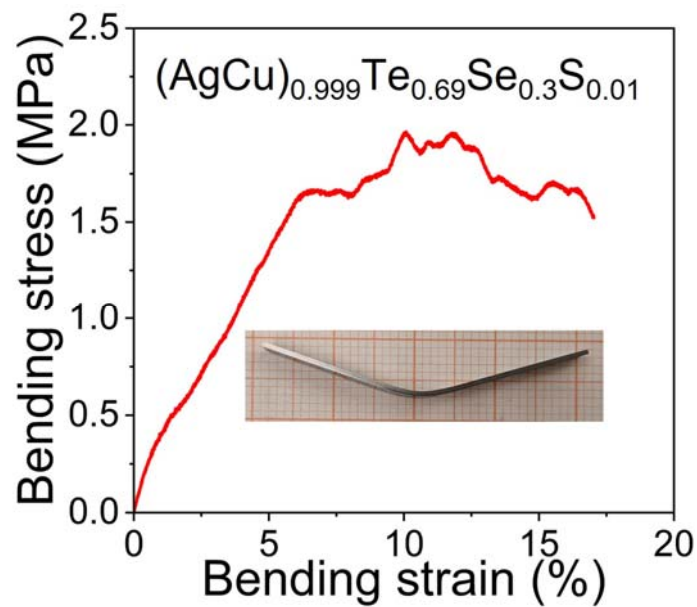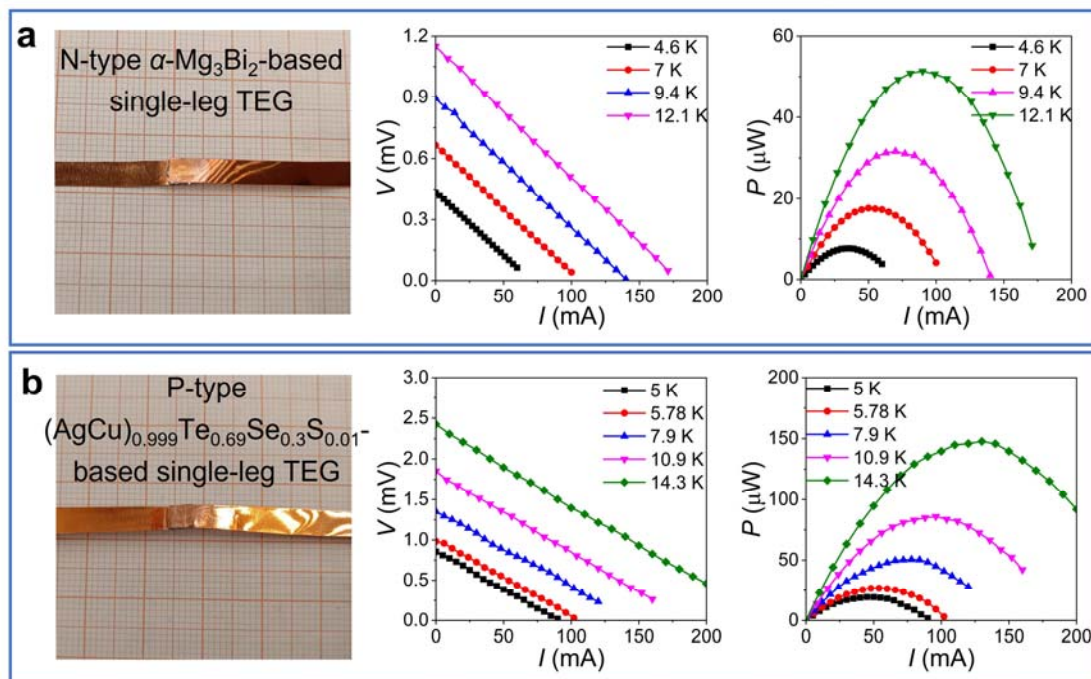
Fig. R17. a, N-type α-Mg$_3$Bi$_2$-based single-leg TEG, and its output performance. **b**, P-type (AgCu)$_{0.999}$Te$_{0.69}$Se$_{0.3}$S$_{0.01}$-based single-leg TEG, and its output performance.

Comment 3. Please provide full details of the thermal conductivity measurements, including uncertainties. "The thermal conductivity was calculated by the fomula of $\kappa = DC_p\rho$, where the thermal diffusivity (D) was tested by Netzsch LFA 467 LT." How was C_p determined?

Response: Thank you for your question. In our paper, the heat capacity was obtained to be 0.254 J g^{-1} K^{-1} from Xin' work [Materials Today Physics 7, 61-68 (2018)], as shown in Fig. R18.

[Figure redacted]

Fig. R18. Temperature dependence of specific heat capacity of Mg$_3$Sb$_2$ and Mg$_3$Bi$_2$ single crystals. These results refer to Xin' work [Materials Today Physics 7, 61-68 (2018)].

Comment 4. There is a concept confusion (also occurring in some parts of the literature), and a few inaccuracies. These points should be polished. "Plasticity" or "Ductility" means that the materials deform permanently (plastically) without fracture or cracking, i.e., ductility is the opposite of brittleness. Please do not confuse "plasticity" and "ductility" with mechanical flexibility, which means that the materials deform elastically (or quasielastically), and then revert to their original shape when the load is removed. This is different from a ductile material, which deforms permanently. Thus, if the material is deforming plastically, it should not be described as mechanically flexible. I believe that the explanation is that the material is indeed mechanically plastic,

but the deformation remains in the elastic part of the stress-strain curve.

Response: Thanks for your valuable suggestions. Plasticity is a broader concept that refers to the ability of a material to undergo irreversible deformation after exceeding its elastic limit. Plasticity encompasses the material's ability to deform under various types of stress, such as tensile, compressive, and shear stress. Ductility is a specific form of plasticity, referring to the material's ability to stretch and undergo plastic deformation under tensile stress. Highly ductile materials can be elongated without fracturing, such as metals being drawn into thin wires. In this work, α-Mg$_3$Bi$_2$ crystals exhibit plasticity but do not possess high ductility. Elasticity refers to the property of an object to undergo deformation under an applied external force and return to its original size and shape once the external force is removed. In this work, α-Mg$_3$Bi$_2$ crystals exhibit a short elastic deformation, according to the mechanical property tests.

In Peng' studies [Science **366**, 690-691 (2019); Matter **4**, 2694-2696 (2021)], flexibility [$f = 1/r = (2/h)(\sigma/E)$, where r is the minimum bending radius of curvature, h is the thickness of materials, σ is yield stress, and E is elastic (Young's) modulus.] is most simply demonstrated by bending a material along a radius of curvature without breakage. Flexible materials need to be compliant (small elastic modulus) and strong (high yield strength), as opposed to stiff and weak. In this work, the α-Mg$_3$Bi$_2$-based out-of-plane flexible thermoelectric generator (f-TEG) showed great flexibility. We subjected the device to repeated bending tests to evaluate the service stability of the TEG devices under different bending radius and bending times. The internal resistance (R_{in}) of f-TEG showed small change under varied bending radius (from 15 mm to 50 mm), and the value of $\Delta R_{in}/R_{in},0$ was less than 7% after bending 2000 times under a bending radius of 15 mm, as shown in Supplementary Fig. 32. Moreover, the output performance also exhibited small change even after repeated bending times of 2000 in Supplementary Fig. 33.

Comment 5. Avoid describing the materials as "plastic semiconductor" and any variation. "Plastic" here is easily misunderstood as "polymer" (which of course would make no sense). Use "ductile" or "mechanically flexible" instead, depending on what is meant.

Response: Thanks for the reviewer's suggestions. In this work, for α-Mg$_3$Bi$_2$ crystal,

"Ductility" and "mechanical flexibility" do not accurately describe material's mechanical properties. To address this ambiguity, the term "plastic semiconductor" has been revised to "plastic inorganic semiconductor", originating from a literature [Joule 8, 1-13 (2024)].

Comment 6. The background and context of the work is generally accurate. However, In the introduction, recent reviews on flexible thermoelectrics should be mentioned,(say, Du et al "Flexible thermoelectric materials and devices" Applied Materials Today 12, 366 (2018) and Wang et al Flexible Thermoelectric Flexible Thermoelectric Materials and Generators: Challenges and Innovations, Advanced Materials 31, 1807916 (2019)). For Mg3Bi2, Sadowski et al. Appl. Phys. Lett. 120, 051901 (2022) might also be relevant.

Response: Thank you for bringing these references to our attention. We have thoroughly read them, cited them in our manuscript, and made adjustments to the main text accordingly.

Comment 7. Furthermore, it is essential to reference also earlier, original, key work on flexible fully inorganic thermoelectrics. For example, ductile/flexible AgS (Nature Materials 2018 and several follow up papers from the same group), CuI (Yang et al, Nature Communications 2017), Ca3Co4O9-based [Paul et al ACS Applied Materials & Interfaces 9, 25308 (2017) and ACS Applied Energy Materials 1, 2261 (2018), as well as several later papers by the same groups], and several CNT-composites (eg Nature Materials 2019, or the review by Blackburn et al Adv. Mater. 30 (2018) 1704386.).

Response: Thank you for bringing these references to our attention. We also have thoroughly read them, cited them in our manuscript, and made adjustments to the main text accordingly.

Mg_3Bi_2 is a very promising material for thermoelectrics. In this article, the authors demonstrate outstanding mechanical properties of Mg_3Bi_2 in terms of plasticity and deformability that is uncommon for inorganic semiconductors. This property is very relevant for the development of flexible (possibly wearable) thermoelectric generators (TEG) as the authors demonstrate themselves by fabricating a flexible TEG with a normalized power density of 8.1 uW/cm$^2 \cdot$K^2 at a temperature difference of 7.3 K.

The study is well-conducted providing a thorough insight into the atomistic nature of the plasticity of Mg_3Bi_2 combining high-resolution microscopy and theoretical calculations.

I therefore think that the article is suitable for publication in Nature Communications, after considering the following aspects:

Response: We would like to thank reviewer 3 for his/her much appreciating our work, and for the comments and suggestions as well. We have carefully taken the comments into consideration in preparing our revision.

Comment 1. It is well-known, and the authors also highlight it in their manuscript, that the stoichiometry (Mg-rich or Bi-rich) greatly affects the electrical properties of Mg_3Bi_2 (n-type or p-type). Does it also have an effect on the mechanical properties? I could not find whether the investigated mechanical properties are on Mg-rich or Bi-rich crystals. What is the stoichiometry of the different crystals employed?

Response: Thank you for your valuable suggestions. In this work, α-Mg_3Bi_2 crystals were grown to obtained the high-performance n-type and p-type samples by the modified Bridgman method with an Mg-excess and Bi-excess conditions, respectively. Excess fluxes (Mg or Bi) tended to concentrate at the top of the samples, and both XRD patterns and Laue backscatter spectra of the main crystalline part matched with the α-Mg_3Bi_2 phase [PDF#04-0464], and indicated the absence of any second phase in α-Mg_3Bi_2 crystals. These indicate that the main parts of both n-type and p-type crystals belong to the room-temperature Mg_3Bi_2 phase.

And as shown in Fig. R19, the n-type Te-doped α-Mg_3Bi_2 crystal also exhibited a bending strain greater than 30%, similar to p-type α-Mg_3Bi_2 crystal, which fully meets

the requirements for the fabrication of f-TEG. Our α-Mg$_3$Bi$_2$-based f-TEG exhibited good the service stability under different bending radius and bending times, as shown in Supplementary Figs. 32 and 33.
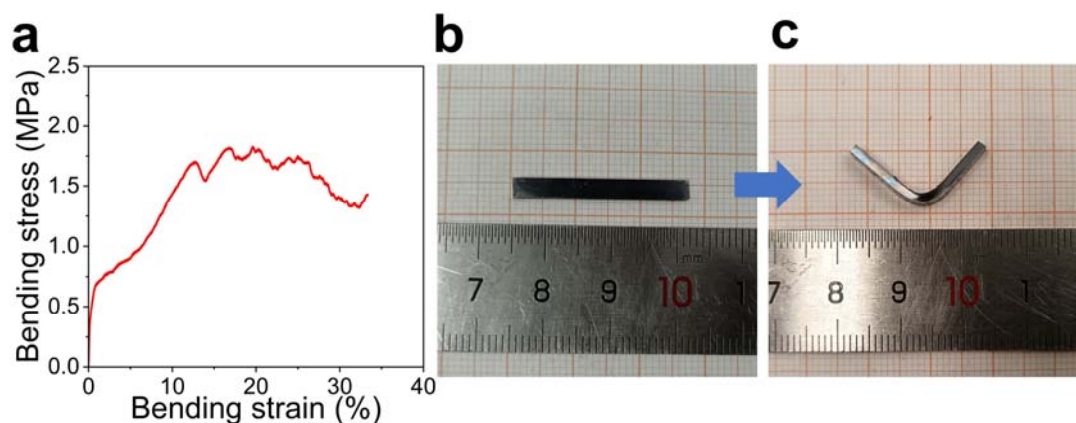

Fig. R19. a. The stress-strain curves of three-point bending test for n-type Te-doped α-Mg$_3$Bi$_2$ crystal. Samples before (**b**) and after (**c**) three-point bending tests.

Comment 2. The authors visualize microstrain induced by bending with atomic-resolution imaging (Figure 2). I wonder whether this would be visible by more-accessible techniques like powder XRD (peak broadening)?

Response: Thanks for your valuable suggestions. Wei et al. compared the XRD patterns of InSe crystal flakes before and after rolling. Both *in situ* SEM compression tests and XRD patterns suggested the (10L) slip planes. Hence, it is the interlayer gliding and cross-layer dislocation slip that enable the exceptional plasticity of bulk InSe single crystals [Science 369, 542-545 (2020)]. In this work, comparing the XRD patterns before and after bending of α-Mg$_3$Bi$_2$ flakes, (10$\bar{1}$L) diffraction peak appeared, which could suggest prismatic slip planes $\{10\bar{1}0\}$. However, we thought this may not be an accurate interpretation. The cleavage planes of α-Mg$_3$Bi$_2$ have numerous layers. When the flakes were repeatedly bent, these layers may be also slightly folded, eventually affecting the XRD results. In this work, we used several direct methods to observe the slip process at the micro and nanoscale. SEM observations revealed extensive interlayer slipping in the deformed samples. In situ SEM also allowed us to observe dynamic interlayer slip process. TEM directly captured helical dislocation-driven interlayer slip

24

induced by strain at nanoscale. What's more, we simulated the slip process by using DFT calculations. The resulting slipping energy (0.04184 eV/atom) and cleavage energy (0.13051 eV/atom) indicated that the low slip energy suggests interlayer slip is highly facile.
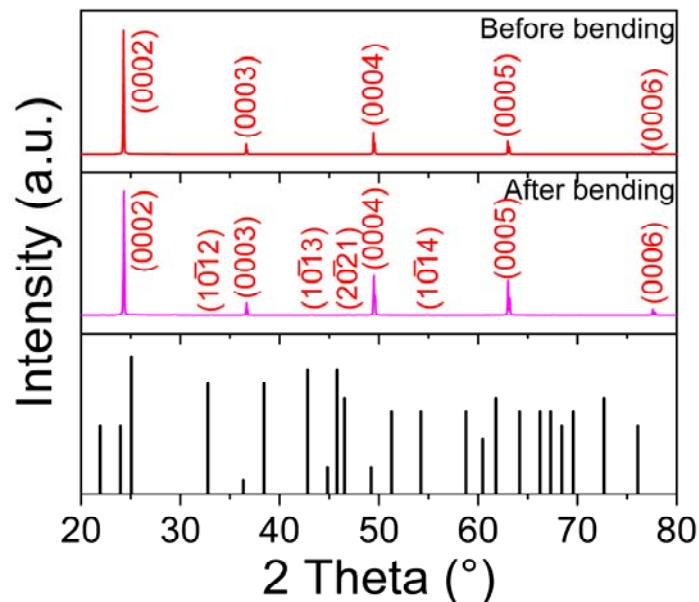

Fig. R20. XRD patterns of α-Mg$_3$Bi$_2$ crystal flakes before and after bending.

Comment 3. For the fabrication of the f-TEG the authors cut "thin plates" from the single crystals, that are around 330 microns thick. In literature, there are several reports on thin films (sub-micron) grown by sputtering or thermal evaporation. How does the thickness affect the thermoelectric and mechanical properties of the material?

Response: Thanks for your valuable suggestions. The size effect in low-dimensional thermoelectric materials play an important role in thermoelectric performance through the quantum confinement effect and interface scattering mechanisms [npj Quantum Materials **1**, 16028 (2016)]. In low-dimensional materials, when the characteristic length of a material in certain direction becomes comparable to the effective de Broglie wavelength of carriers, the motion of carriers is restricted in certain directions, which means that carriers are placed in the potential wells with infinitely high walls. In this case, the electronic spectrum will be drastically changed. Quantum confinement effect can enhance thermoelectric performance by improving the Seebeck coefficient through

25

an increase in the electronic density of states. While quantum confinement effect can also lead to a strong modification of phonon group velocities and a significant increase in the phonon relaxation rates, thus reducing the thermal conductivity. With the reduced dimensionality of materials, the possibility of interface scattering of phonons increases. When the phonon mean free path is comparable to the characteristic length of interfaces, significant phonon scattering by interfaces can be expected, which has a significant effect on the lattice thermal conductivity [npj Quantum Materials **1**, 16028 (2016)]. The quantum confinement effect plays a crucial role in designing high-performance thermoelectric materials. In 2001, Rama Venkatasubramanian' work prepared a p-type Bi_2Te_3/Sb_2Te_3 superlattices with a high zT at 300 K of ~2.4 by controlling the transport of phonons and electrons in the superlattices [Nature **413**, 597-602 (2001)].

In flexible electronics field, flexible organic/inorganic thermoelectric hybrids (sub-micron) play a very important role. Typically, their thermoelectric performance is influenced by size effect. In the literature [Advances in Materials Science and Engineering **2019**, 6954918 (2019)], Sb_2Te_3 thin films with various thicknesses (384-1804 nm) were deposited on a flexible substrate using RF magnetron sputtering. As the film thickness increased, the grain size also increased. The increase in the mean free path of carriers due to grain size enhanced the electrical conductivity and power factor of Sb_2Te_3 thin films. The mechanism of thermal conductivity was explained by the Callaway model [Phys Rev. **113**, 1046 (1959)]

$$\kappa_L(T) = \frac{k_B}{2\pi^2 c}\left(\frac{k_B T}{\hbar}\right)^3 \int_0^{\theta_D/T} \tau_c \frac{x^4 e^x}{(e^x - 1)^2} dx \qquad (R7)$$

The total modified phonon scattering rate (relaxation time, τ_c) was adapted to be [Nanoscale Research Letters **10**, 20 (2015)]

$$\tau_c^{-1} = \frac{c}{d_1} + \frac{c}{d_2} + A\omega^4 + B\omega^2 T exp\left(-\frac{\theta_D}{3T}\right) + C\omega \qquad (R8)$$

where d_1 is the grain size of the thin films, d_2 is the film thickness, c is average sound velocity from bulk Sb_2Te_3. The first term, c/d, represents boundary scattering; the second term, $A\omega^4$, represents point-defect scattering; the third term, $B\omega^2 T exp(-\theta_D/3T)$, represents three-phonon Umklapp scattering, while the fourth term, $C\omega$, represents carrier phonon scattering. The thermal conductivity related to phonon or carrier

scattering. For film thickness less than 1 μm, the phonon scattering is dominant, while both are dominant for film thickness above 1 μm. Finally, the zT value of Sb_2Te_3 thin film reached maximum at 1 μm [Advances in Materials Science and Engineering **2019**, 6954918 (2019)]. The same phenomenon occurs in other material systems. In literature [*Adv. Mater.* **34**, 2104786 (2022)], Ag_2Se thin films (550-1600 nm) were prepared by a room-temperature aqueous selenization reaction. The morphology (e.g. grain size or texture) of Ag_2Se thin films varied with different thicknesses, which caused that the thermoelectric performance (e.g. carrier concentration, electric conductivity, power factor, zT value) Ag_2Se thin films also varied with different thicknesses by the size effect.

In this work, the 330 μm α-Mg_3Bi_2 thick plates (4×4 mm^2) were cut to fabricate f-TEG by using the diamond wire cutting. In the cutting process, structure and morphology of crystals remained unchanged. The longitudinal v_l and transverse sound velocities v_t are 3248 and 1796 m/s, respectively, for α-Mg_3Bi_2 [Appl. Phys. Lett. **123**, 252109 (2023)]. The phonon lifetime of α-Mg_3Bi_2 is located at 10^{-1}-10 ps [Appl. Phys. Lett. **123**, 252109 (2023); Nanomaterials **13**, 2938 (2023)]. According to the formulas R7 and R8, the thickness of 330 μm have no effect on the relaxation time and thermal conductivity for α-Mg_3Bi_2. This is supported by numerous studies in the literature. As shown in Fig. R21, coarse-grained polycrystalline samples of tens of μm are preferred to have a similar TE performance to the single crystals with the same composition. According to the formulas R7, for α-Mg_3Bi_2, the lattice thermal conductivity of fine-grained polycrystalline samples of tens of nm could be affected by size effect. And the carrier mobility of polycrystalline samples at room temperature tends to have a slower increase when the grain size reaches above ~10 μm. And the 330 μm thickness is much larger the electron mean free path (~10 nm) [Chemical Engineering Journal **490**, 151404 (2024)], which means that the carrier transport process couldn't be affected by quantum size effects. In conclusion, quantum confinement effect and interface scattering effect have no effect on the thermoelectric performance of the 330 μm α-Mg_3Bi_2 thick plates, which have the same thermoelectric performance as bulk α-Mg_3Bi_2 crystal.

[Figure redacted]

Fig. R21. The carrier mobility (μ_H) and lattice thermal conductivity (κ_L) at room temperature versus grain size for $Mg_3(Sb, Bi)_2$ solid solutions [Research **2020**, 1934848 (2020)].

When fabricating f-TEGs, thin and small thermoelectric legs are preferred to ensure device flexibility [Science 377, 854-858 (2022), Nat. Commun. 15, 5108 (2024)], which is crucial for applications that require bending and stretching. And, flexibility of materials is ensured by reducing the material's stiffness through control of its thickness and dimensions [Science **366**, 690-691 (2019)]. Stiffness refers to the resistance of an object or structure to deformation under an external force. And stiffness is commonly used in mechanical systems to quantify the amount of deformation resulting from a unit external force. Stiffness is a structural property, which is closely influenced by the geometry, size, and material characteristics of the object. The material's stiffness (K) can be calculated by the formula ($K=EA/L$), where E is the elastic modulus, and A and L are the cross-sectional area and length, respectively [Introduction To Solid Mechanics - Irving H. Shames, James M Pitarresi, 2003]. When the material' cross-sectional area (thickness and width) decreases, its stiffness also decreases, while its flexibility increases. That is why f-TEGs require thin and small thermoelectric legs to maintain device flexibility.

REVIEWERS' COMMENTS

Reviewer #1 (Remarks to the Author):

I want to thank the authors for providing detailed answers and making the additional calculations in the revised manuscript. Almost all my requirements have been satisfied. I believe that the content of this manuscript has been improved; in particular, the authors have clarified the role of the iDPC method compared with the TEM method in the previous publications and also performed the AIMD simulations to understand the atomic structure. Thus, I suggest publishing this work as it is on Nat. Commun.

Response: Thank you for the positive comment.

Reviewer #2 (Remarks to the Author):

The authors have addressed all comments from the three reviewers in a very thorough and complete manner. I am pleased to recommend this paper for publication in Nature Communications.

Response: Thank you for the positive comment.

Reviewer #3 (Remarks to the Author):

The authors have appropriately answered all my previous comments. I have no further comments and recommend publication of the current manuscript.

Response: Thank you for the positive comment.